




Article

Influence of the Shrinkage of the Inner Layer of Steel Tubes on Permissible Thermal Load

Mateusz Zieliński * , Piotr Koniorczyk  and Zbigniew Surma 

Faculty of Mechatronics, Armament and Aerospace, Military University of Technology, 2 gen. S. Kaliskiego Street, 00-908 Warsaw, Poland; piotr.koniorczyk@wat.edu.pl (P.K.); zbigniew.surma@wat.edu.pl (Z.S.)

* Correspondence: mateusz.zielinski@wat.edu.pl; Tel.: +48-261-839-647

Abstract: This paper presents the results of numerical simulations of heat transfer in a tube with a protective chromium layer on the inner surface made of steel, with different shrinkage temperatures. Shrinkage in the steel is an unfavorable phenomenon because it causes cracks in the chrome coating. The cracks contribute to the peeling of the protective material on the inner surface of the tube. Wear and damage to the chrome layer significantly shortens the tube's service life. The influence of the type of steel with medium carbon content on heat transfer for a sequence of ten, thirty, and sixty heat impulses was examined. Simulations were carried out for two selected steels with clearly different shrinkage temperatures, i.e., 30HN2MFA and X37CrMoV5-1 (1.2343). In 30HN2MFA steel, the shrinkage effect occurred at a temperature of approx. 750 °C, while in X37CrMoV5-1 steel it occurred at a temperature of approx. 870 °C. In the computational model, 30 cross-sections of the three-meter-long tube were analyzed. A time-dependent heat transfer coefficient was calculated in each zone. Heat transfer simulations were carried out using COMSOL version 6.1 software. This paper shows that for X37CrMoV5-1 steel, the shrinkage temperature on the inner surface of the tube was reached after approx. 60 heat impulses, while for 30HN2MFA steel, it was reached after approx. 30. The greatest differences in the number of impulses occurred for a pipe with a 200 μm thick chrome layer.

Keywords: heat transfer; temperature field; protective coating; shrinkage of the steel; modeling



Citation: Zieliński, M.; Koniorczyk, P.; Surma, Z. Influence of the Shrinkage of the Inner Layer of Steel Tubes on Permissible Thermal Load. *Energies* **2024**, *17*, 702. <https://doi.org/10.3390/en17030702>

Academic Editor: Paulo Santos

Received: 8 January 2024

Revised: 25 January 2024

Accepted: 31 January 2024

Published: 1 February 2024



Copyright: © 2024 by the authors. Licensee MDPI, Basel, Switzerland. This article is an open access article distributed under the terms and conditions of the Creative Commons Attribution (CC BY) license (<https://creativecommons.org/licenses/by/4.0/>).

1. Introduction

The durability of tube bores in which gas flows at high pressure (of the order of hundreds of MPa) and high temperature (of the order of thousands of Kelvin) is influenced by mechanical erosion and changes in the thermophysical properties of steel. Papers [1,2] discuss the mechanism related to the mechanical and thermal erosion of internal tubes. These papers describe several causes of erosion. They indicate that one of the causes of the cracking of chrome layers is the change in the volume of the substrate under the influence of high temperatures. This mechanism involves pressing the steel substrate on the chrome layer when it is heated to 730 °C. The pressure on the chrome layer is caused by the thermal expansion of the steel substrate. In papers [1,2], the issue of crack formation due to phase transformation in steel is only mentioned. A zone under the influence of high temperatures are called "heat-affected zone" [1–3]. Direct indications that the ferrite-austenite phase transformation causes the formation of cracks on the inner surface of the tube can be found in papers [4–6]. These works determined that this phenomenon occurs at temperatures above 750 °C. The cyclic heating and cooling of the tube cause volume changes that lead to subsurface stresses, resulting in the formation of cracks. The resulting cracks in the steel layer also cause the cracking of the chrome layer [5]. Similar effects are shown in [7]. In this study, a chromium layer was annealed on a 416 stainless steel substrate. The authors of publication [7] examined the appearance of cracks in the chrome layer by heating it to 600 °C and 800 °C, respectively. At a temperature of 600 °C, no cracks

were observed, while at the second temperature, cracks in the chrome layer were visible. According to the authors of work [7], this effect is related to the different values of the thermal expansion coefficient for the chrome layer and steel 416. It should be noted that the authors of work [7] performed measurements at temperatures 50 °C lower and higher than the phase transformation temperature presented in works [4–6]. Based on the chemical composition of 416 stainless steel [7] and steel of similar composition and properties [8], it can be assumed that the phase transformation for this steel also occurs in the temperature range of 600–800 °C. The shrinkage effect caused by the allotropic transformation was observed in the steels described in works [9,10]. In the case of alloy steels, the shrinkage temperature causing cracking can range from 750 °C to 870 °C [10–12]. For example, the depth of cracks in a 30HN2MFA steel tube can be up to 0.3 mm [13].

Shrinkage in the wall of the tube is an unfavorable phenomenon because the cracks contribute to the peeling of the protective coating (e.g., chromium or nitride layer) on the inner channel. Wear and damage to the chrome layer significantly shortens the tube's service life. An analysis of permissible thermal load cycles is presented in [14,15]. These works indicate the need to use breaks between subsequent series of thermal loads. Sufficiently long breaks can prevent the steel from reaching the shrinkage temperature. However, in works [16–18], the length of the series of thermal impulses that causes the shrinkage temperature to be reached was determined. The analyzes were performed for various steel grades.

Taking the above into account, it seems advisable to investigate the effect of shrinkage temperature on the permissible length of a series of thermal impulses. Such analysis can be carried out through heat transfer calculations [19–25]. Only after simulating dozens of heat impulses is the shrinkage temperature of the material reached.

2. Materials and Methods

In this paper, the heat transfer in a pipe without a chrome layer and with a protective coating of chromium on its inner surface with a thickness of 30 µm and 200 µm, was solved for the sequence of ten, thirty, and sixty heat impulses. Calculations were performed for the two selected steels with clearly different shrinkage temperatures, i.e., 30HN2MFA and X37CrMoV5-1 (1.2343). In 30HN2MFA steel, the shrinkage effect occurred at a temperature of approx. 750 °C, while in X37CrMoV5-1 steel, it occurred at a temperature of approx. 870 °C. The model of the tube with an overall length of 3150 mm and 35 mm inner channel is presented in Figure 1. The gas temperature, $T_g(t)$, and the heat transfer coefficient, $h_i(t)$, were determined for 30 cross-sections (P1 to P30—see Table 1), using the method described in [17,18]. The results of the calculations for cross-section P_i are applicable to the entire length of the S_i zone. For the calculations, the parameters of selected steels and galvanic chromium (Cr) as functions of temperature from [10,26–29] were assumed. As part of this investigation, for each selected steel, the number of heat impulses necessary to reach the shrinkage temperature was calculated. To sum up, the more heat impulses are needed for the steel to reach the shrinkage temperature, the later the formation and propagation of cracks on the inner surface of the pipe, and, consequently, cracks and damage to the chrome coating will occur.

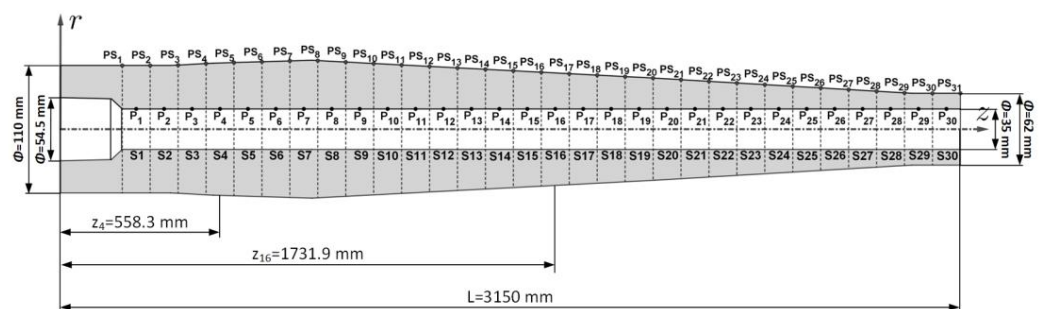


Figure 1. Geometry and division of the tube into zones.

Table 1. Geometrical parameters of the tube zones: PS_i —zone boundaries; R_{out,PS_i} —outer radius in zone boundary i ; z_i —distance from the bottom of the tube to the cross-section P_i in the middle of zone S_i . Data from [18].

Number of Zone i	S1	S2	S3	S4	S5	S6	S7	S8	S9	S10
PS_i [mm]	216.0	313.8	411.6	509.4	607.2	705.0	802.8	900.6	998.4	1096.2
R_{out,PS_i} [mm]	55.00	55.00	55.35	55.66	57.52	58.23	58.94	59.24	57.94	56.72
z_i [mm]	264.9	362.7	460.5	558.3	656.1	753.9	851.7	949.5	1047.3	1145.1
Number of Zone i	S11	S12	S13	S14	S15	S16	S17	S18	S19	S20
PS_i [mm]	1194.0	1291.8	1389.6	1487.4	1585.2	1683.0	1780.8	1878.6	1976.4	2074.2
R_{out,PS_i} [mm]	55.47	54.21	52.93	51.70	50.44	49.18	47.93	46.67	45.41	44.16
z_i [mm]	1242.9	1340.7	1438.5	1536.3	1634.1	1731.9	1829.7	1927.5	2025.3	2123.1
Number of Zone i	S21	S22	S23	S24	S25	S26	S27	S28	S29	S30
PS_i [mm]	2172.0	2269.8	2367.6	2465.4	2563.2	2661.0	2758.8	2856.6	2954.4	3052.2
R_{out,PS_i} [mm]	42.75	41.33	39.90	38.48	37.06	35.64	34.22	32.79	31.37	31.00
z_i [mm]	2220.9	2318.7	2416.5	2514.3	2612.1	2709.9	2807.7	2905.5	3003.3	3101.1
PS_{31} [mm]	3150									

In devices of this type, heat is transferred mainly through convection from the gas of the heat impulse. The heat flux density on the inner surface of the tube reaches hundreds of millions of W/m^2 at the moment of a heat impulse [17]. Due to the very short impulse duration, we ignore the heat transfer through radiation between the gas and the inner surface of the tube [17]. The $h_i(t)$ and $T_g(t)$ data are taken from [18]. An example of the calculation results of $h_i(t)$ and $T_g(t)$ in the selected cross-sections PS_4 , PS_{10} , PS_{16} , PS_{21} , PS_{25} , and PS_{30} is presented in Figure 2. A detailed method of calculating $h_i(t)$ and $T_g(t)$ is presented in [18].

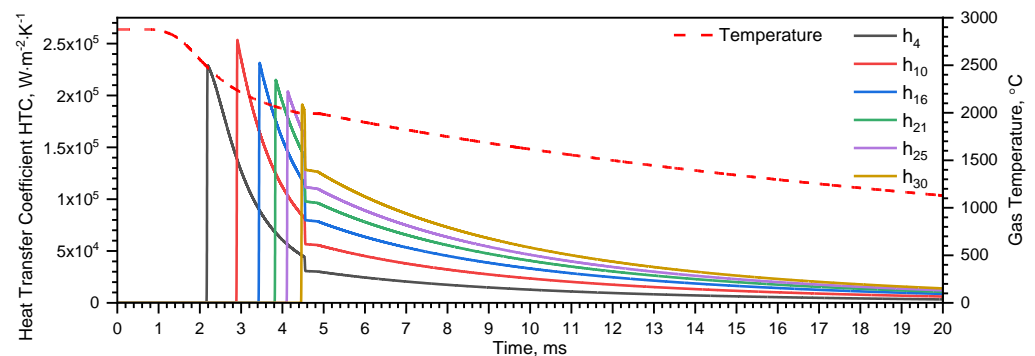


Figure 2. Results of the calculation of h_i and T_g in the chosen zones (i —number of zone). Data from [18].

It should be emphasized that the subject of the analysis in this paper was not the solution of the initial boundary value problem in a tube with a chrome coating on its inner surface, because this problem for a maximum of 7 thermal impulses was presented by the authors in [18]. The same boundary conditions, the same time step, and the same mesh were used in this work. However, two steels with extremely different shrinkage temperatures were selected, i.e., 30HN2MFA and X37CrMoV5-1, and calculations were made for such a number of impulses that the shrinkage temperature was exceeded in both steels. The calculation time for 60 heat impulses increased to 6 h. However, qualitatively new results were obtained, which illustrated the influence of the number of impulses on the thermal load of the tube related to the shrinkage temperature.

The thickness of the chromium layer on the inner surface of the tube, i.e., 30 μm and 200 μm , was selected to take into account the possible thermal contact resistance between the chromium layer and the steel substrate. For such a case, M.M. Yovanovich suggests that the chromium layer must be thicker than 100 μm [30]. Initial numerical simulations of heat transfer, taking into account thermal contact resistance according to the Yovanovich model, led to overestimating the results of temperature calculations on the inner surface of the tube; therefore, thermal contact resistance was ultimately not taken into account.

Thermophysical Properties of Selected Steels with Medium Carbon Content

The temperature-dependent thermal conductivity k_s , specific heat c_s , and density ρ_s of selected steels with medium carbon content, i.e., 30HN2MFA, X37CrMoV5-1, and galvamic chromium, i.e., Cr (Figures 3–5), were adopted as the input data to the heat transfer simulation. The chromium thermophysical properties (k_{Cr} , c_{Cr} , and ρ_{Cr}) were taken from [26–28].

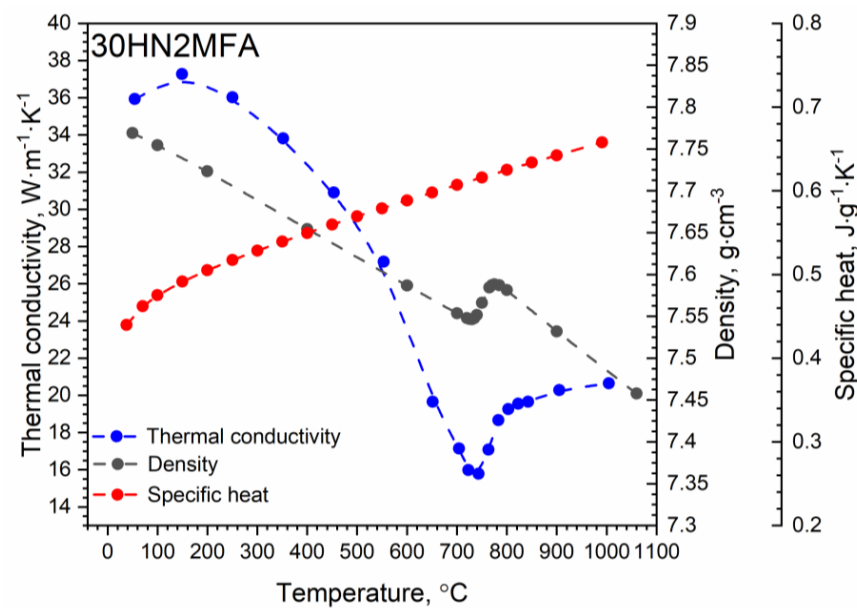


Figure 3. Thermophysical properties of 30HN2MFA steel. Data from [10].

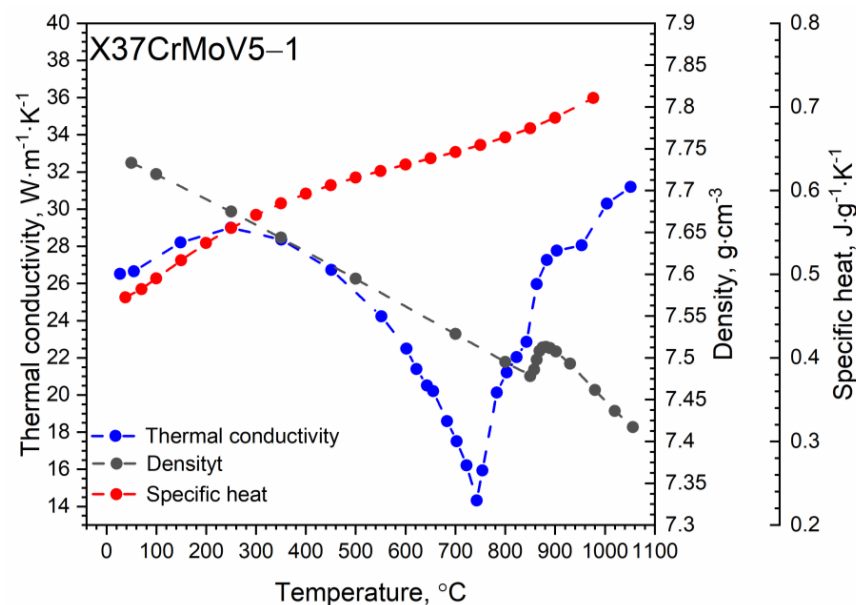


Figure 4. Thermophysical properties of X37CrMoV5-1 steel. Data from [29].

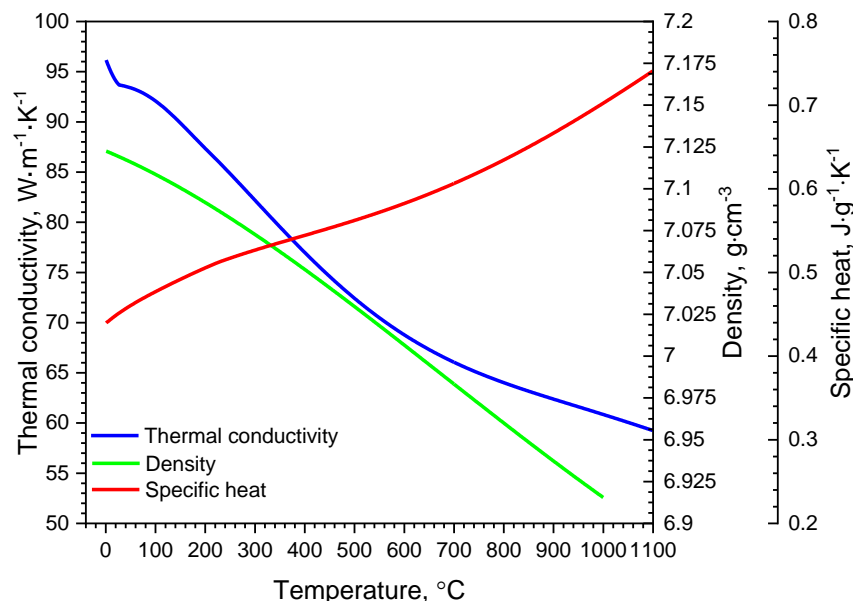


Figure 5. Thermophysical properties of Chromium. Data from [26–28].

The above-mentioned properties of both steels, i.e., high strength steel 30HN2MFA and hot-work tool steel X37CrMoV5-1, were measured by the authors and presented in [10,29]. In our opinion, the shrinkage temperature of the steel depends on the chromium content. According to [29], X37CrMoV5-1 steel with 5.52% chromium content has the highest shrinkage temperature at 870 °C among the tested steels, while 30HN2MFA steel with 0.65% chromium content has the lowest shrinkage temperature at 750 °C. More details on the composition of these steels can be found in Table 2.

Table 2. X37CrMoV5-1 and 30HN2MFA steel—composition. Data from [10,29].

Steel	Composition, (wt. %)							
	Fe	C	Si	Mn	Cr	Mo	Ni	V
30HN2MFA	96.42	0.29	0.26	0.36	0.65	0.24	2.21	0.23
X37CrMoV5-1	90.71	0.39	0.84	0.36	5.52	1.30	0.40	0.45

In our research described in [10,29], it was shown that for 30HN2MFA steel, at a temperature of about 750 °C, and for X37CrMoV5-1 steel, at 870 °C, a ferrite-austenite phase transition occurs which is responsible for the material shrinkage—Figures 3 and 4. The energy associated with the phase transition was included in the thermal conductivity and density of the tested steel. The specific heat of this energy was disregarded. This issue was thoroughly discussed by the authors in [29].

3. Numerical Calculations

The numerical calculations of transient heat transfer in the tube were carried out for the sequence of ten, thirty, and sixty heat impulses. The same numerical method and model was used by the authors in [17,18]. The inner radius r_{in} , the interface radius r_m , and the outer radius r_{out} were defined as shown in Figure 6.

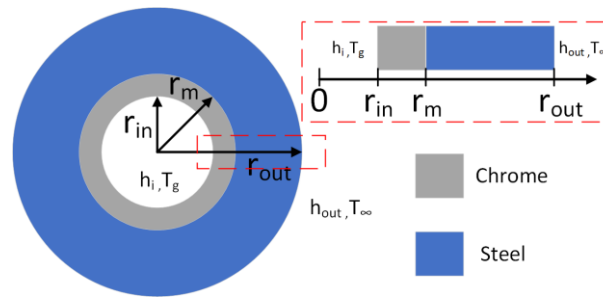


Figure 6. Model of a tube. Data from [18].

The parameters of the steels (30HN2MFA or X37CrMoV5-1) (k_s , c_s , ρ_s) and chromium (k_{Cr} , c_{Cr} , and ρ_{Cr}) were used. Calculations were carried out for the initial temperature of the model $T_0 = 20$ °C and the heat transfer coefficient on the outer surface of $h_{out} = 9.2$ W/(m²·K). According to [17,18], the thermal resistance of the steel–chromium interface was omitted. The main equations of considered heat transfer problem with initial and boundary conditions are as follows:

$$\left. \begin{aligned} \rho_{Cr}(T)c_{Cr}(T)\frac{\partial T}{\partial t} &= \frac{1}{r}\frac{\partial}{\partial r}\left(k_{Cr}(T)r\frac{\partial T}{\partial r}\right) + \frac{\partial}{\partial z}\left(k_{Cr}(T)\frac{\partial T}{\partial z}\right) \\ r_{in} < r < r_m, 0 < z < l_m, t > 0 \end{aligned} \right\} \quad (1)$$

$$\left. \begin{aligned} -k_{Cr}(T)\frac{\partial T}{\partial r} &= \dot{q}_i(t, r = r_{in}, z) \\ \dot{q}_i(t, r = r_{in}, z) &= h_i(t) \cdot (T(t, r_{in}, z) - T_g(t, r_{in}, z)) \\ i &= 1, \dots, 30 \text{ (} i \text{ - a zone number)} \end{aligned} \right\} \quad (2)$$

$$-k_{Cr}(T)\frac{\partial T}{\partial r} = -k_s(T)\frac{\partial T}{\partial r}, T_{Cr} = T_s, r = r_m \quad (3)$$

$$\left. \begin{aligned} \rho_s(T)c_s(T)\frac{\partial T}{\partial t} &= \frac{1}{r}\frac{\partial}{\partial r}\left(k_s(T)r\frac{\partial T}{\partial r}\right) + \frac{\partial}{\partial z}\left(k_s(T)\frac{\partial T}{\partial z}\right) \\ r_m < r < r_{out}, 0 < z < l_m, t > 0 \end{aligned} \right\} \quad (4)$$

$$\left. \begin{aligned} -k_s(T)\frac{\partial T}{\partial r} &= \dot{q}_{out} \\ \dot{q}_{out} &= h_{out} \cdot (T(t, r_{out}, z) - T_0) \end{aligned} \right\} \quad (5)$$

$$T(0, r, z) = T_0, r_{in} < r < r_{out}, 0 < z < l_m \quad (6)$$

where T_g is the gas temperature, $r_{in} = \frac{35}{2}$ mm, r_{out} —Table 1, and l_m is the tube length (see Figure 1).

The numerical model mesh and its validation were performed according to publication [18]. Sensitivity tests of the model mesh were carried out in the same way as in the above publication. The mesh size in the form of quad on the inner surface of the tube had no significant impact on the calculation results. The smallest mesh size used for the calculations was 0.1 μ m. Calculations for the same pipe were previously carried out by another team at our university. Validation was performed by comparing the calculation results of the temperature increase on the outer surface of the pipe in zone 26 under the same conditions [18]. The temperature of the inner surface versus time for a single heat impulse is presented in Figure 7.

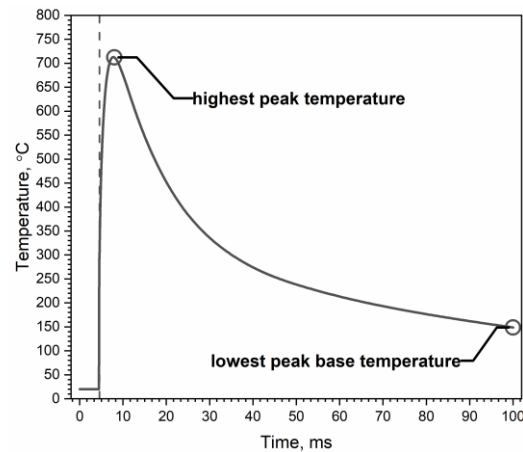


Figure 7. The temperature of the inner surface of the tube versus time for a single heat impulse. Data from [18].

3.1. Temperature Distribution in the 30HN2MFA Tube for a Series of Ten, Thirty, and Sixty Heat Impulses

The thermophysical properties of steels 30HN2MFA and X37CrMoV5-1 were obtained by extrapolating experimental data in the range 1000 °C to 1300 °C. The temperature values $T_i(t, r, z)$ inside the wall of the tube for different chromium layers, i.e., 0, 30, and 200 μm , at zone S30 for the sequence of sixty heat impulses are presented in Figure 8. The temperature of phase transition (750 °C) appears for the tube with different chromium layer thicknesses at different times, the fastest for the barrel with 200 μm Cr. After 2.7 s, i.e., after 27 heat impulses, zone S30 of the tube reaches the phase transition temperature—Figure 8.

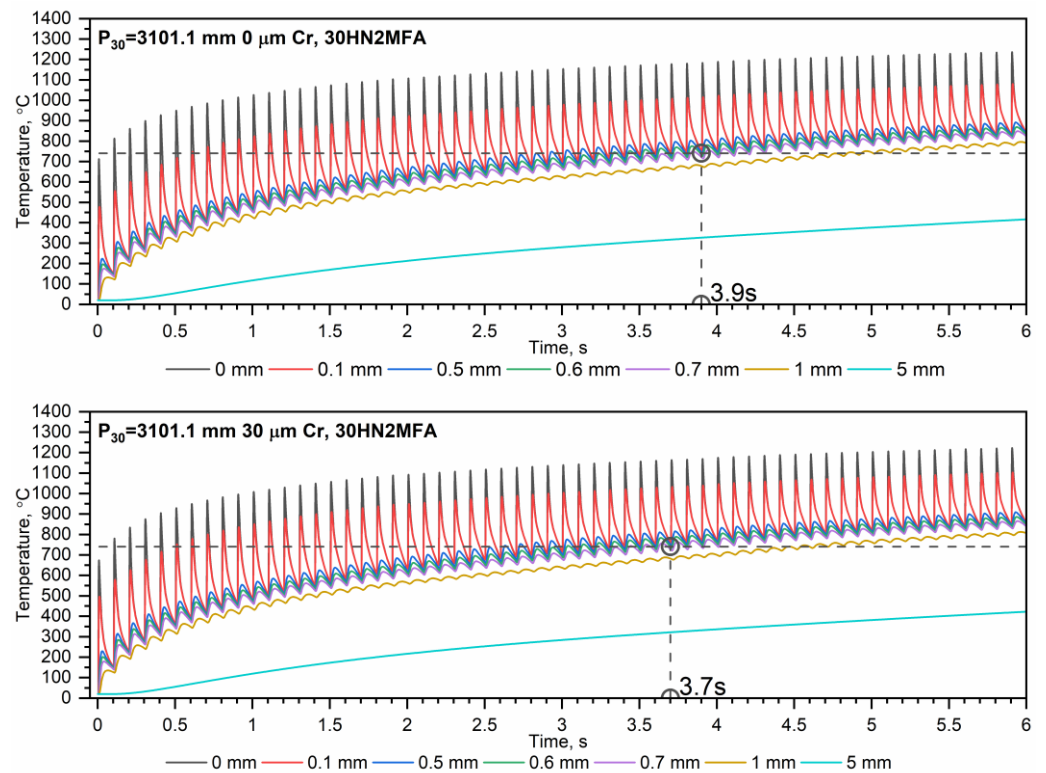


Figure 8. Cont.

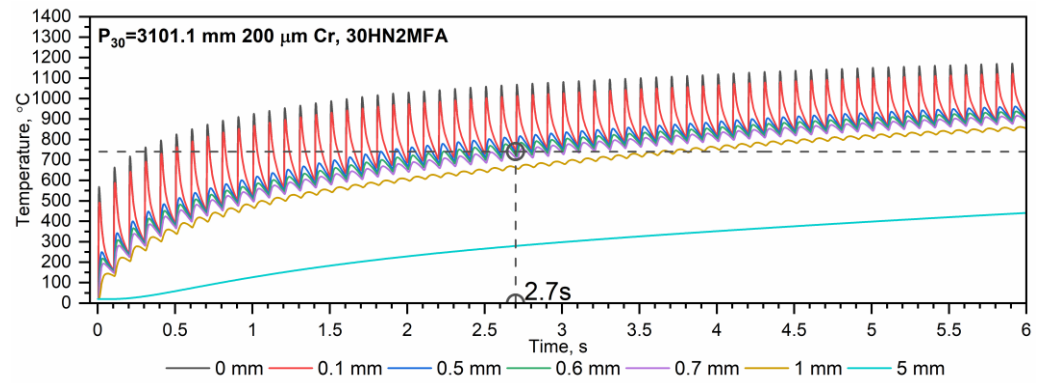


Figure 8. Temperature change $T_i(t, r, z)$ in the S30 zone for a series of 60 heat impulses for different depths from the inner surface of the tube, for 30HN2MFA steel. The coloured lines indicate the depth from the inner surface of the tube according to the graph legend.

The envelopes of the lowest peak temperatures (the bottom curves in each drawing) and the highest peak temperatures (the top curves in each drawing) of the inner surface with different thicknesses of Cr (0, 30, and 200 μm) at the chosen six zones, i.e., S4, S10, S16, S21, S25, and S30, for 60 heat impulses are shown in Figure 9. The selection of zones takes into account the change in the outer diameter of the tube along its length. In zones 4, 10, and 16, the highest peak temperatures are similar, and after 60 heat impulses, they are a little higher than 1300 $^{\circ}\text{C}$, when the temperature in zones 21, 25, and 30 is little below 1300 $^{\circ}\text{C}$. However, for the lowest peak temperatures, in all zones, after 60 heat impulses, the temperatures are close to 850 $^{\circ}\text{C}$.

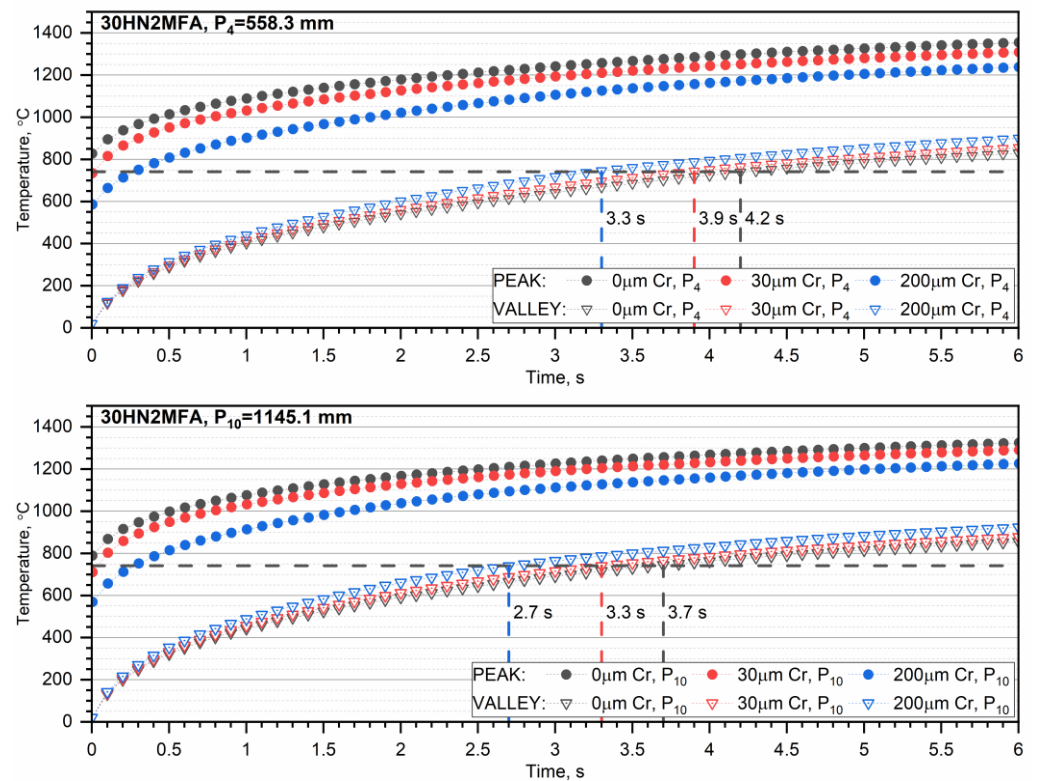


Figure 9. Cont.

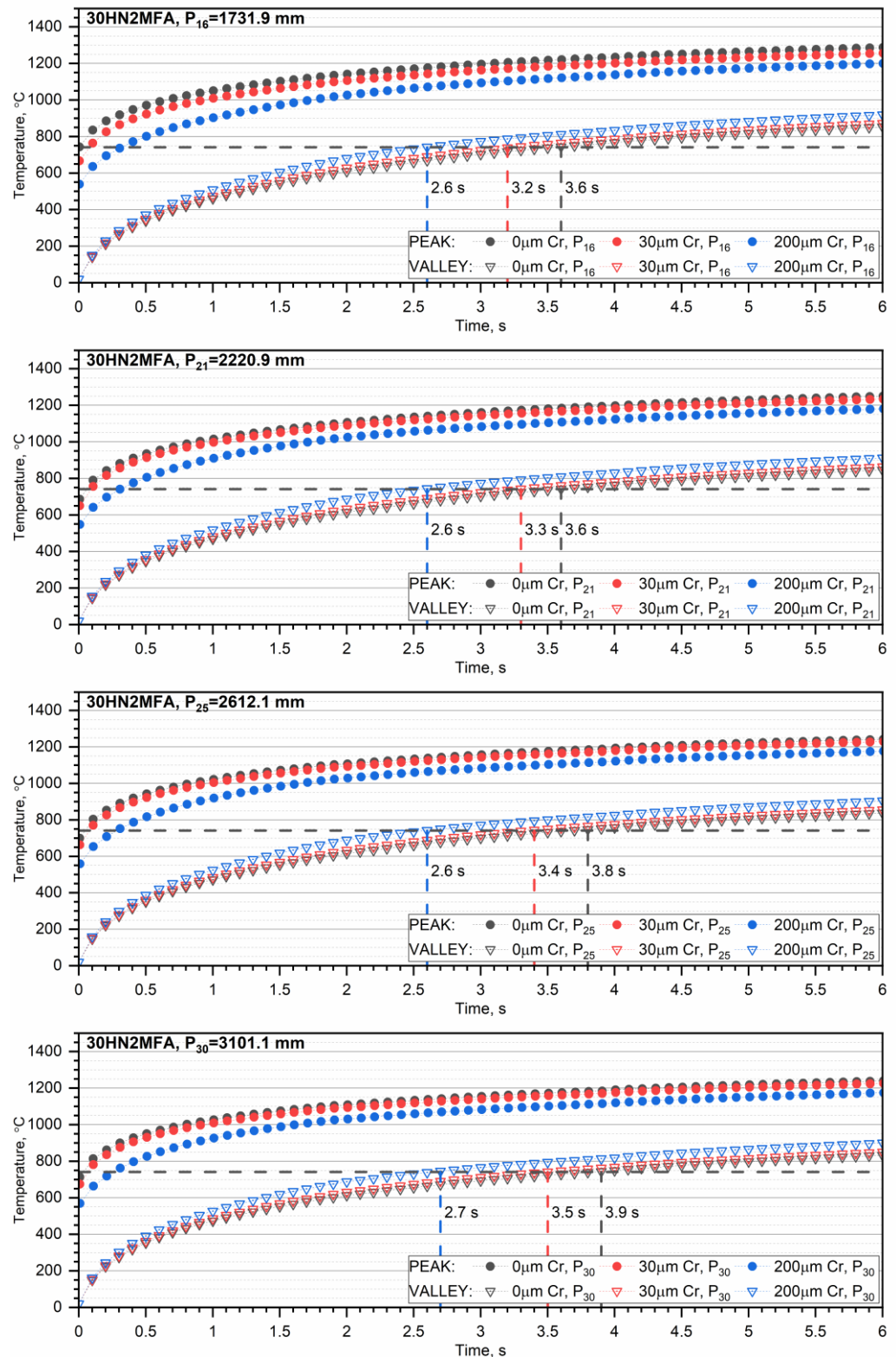


Figure 9. Envelopes of the lowest peak base temperatures (VALLEY) and the highest peak temperatures (PEAK) of the inner surface for 60 heat impulses.

The highest peak temperatures and the lowest peak base temperatures for the considered cross-sections after 10, 30, and 60 heat impulses are presented in Figures 10–12. After 10 heat impulses, the maximum of the lowest peak base temperature is in the S27–S30 zones (Figure 10). After 30 heat impulses, the lowest peak base temperature reaches a maximum

in zones S14–S22 (Figure 11), and after 60 heat impulses, it reaches a maximum in zones S8–S14 (Figure 12).

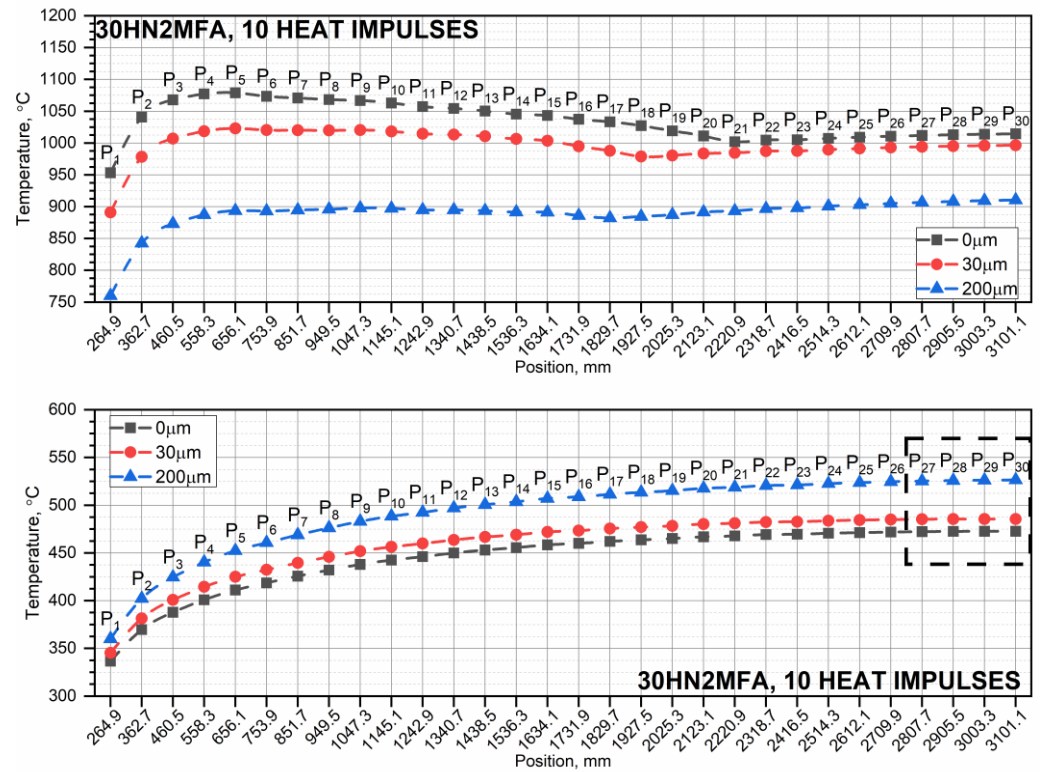


Figure 10. The highest peak temperatures (upper figure) and the lowest peak base temperatures (lower figure) for the considered cross-sections for 10 heat impulses.

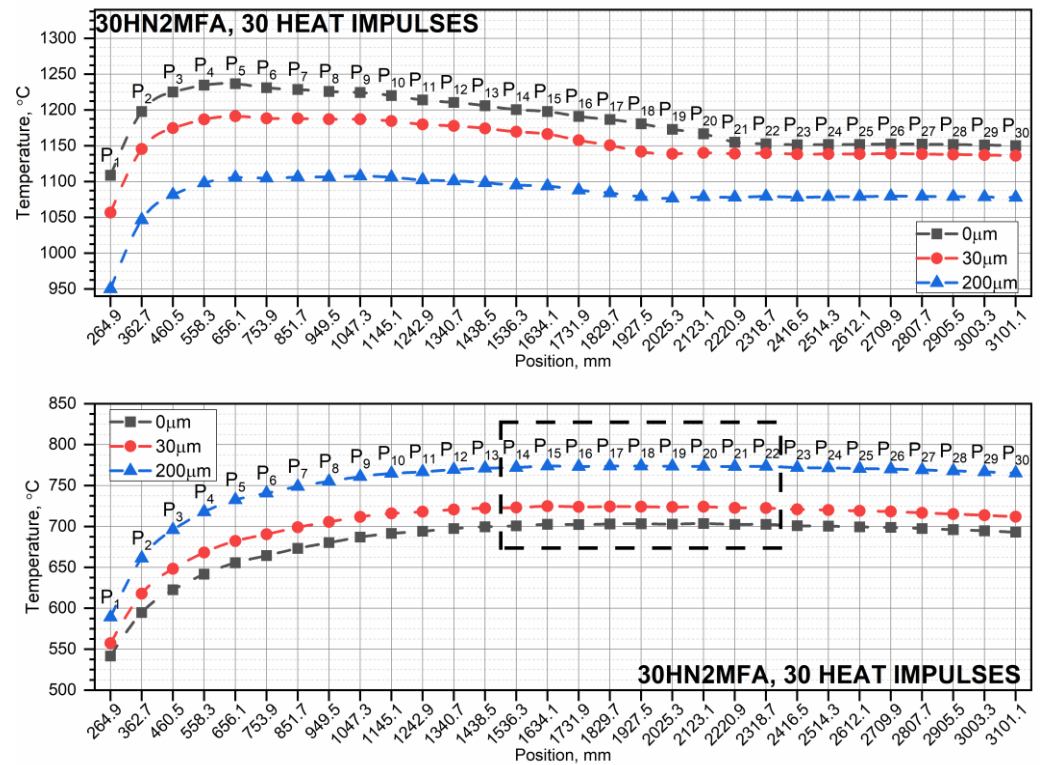


Figure 11. The highest peak temperatures (upper figure) and the lowest peak base temperatures (lower figure) for the considered cross-sections for 30 heat impulses.

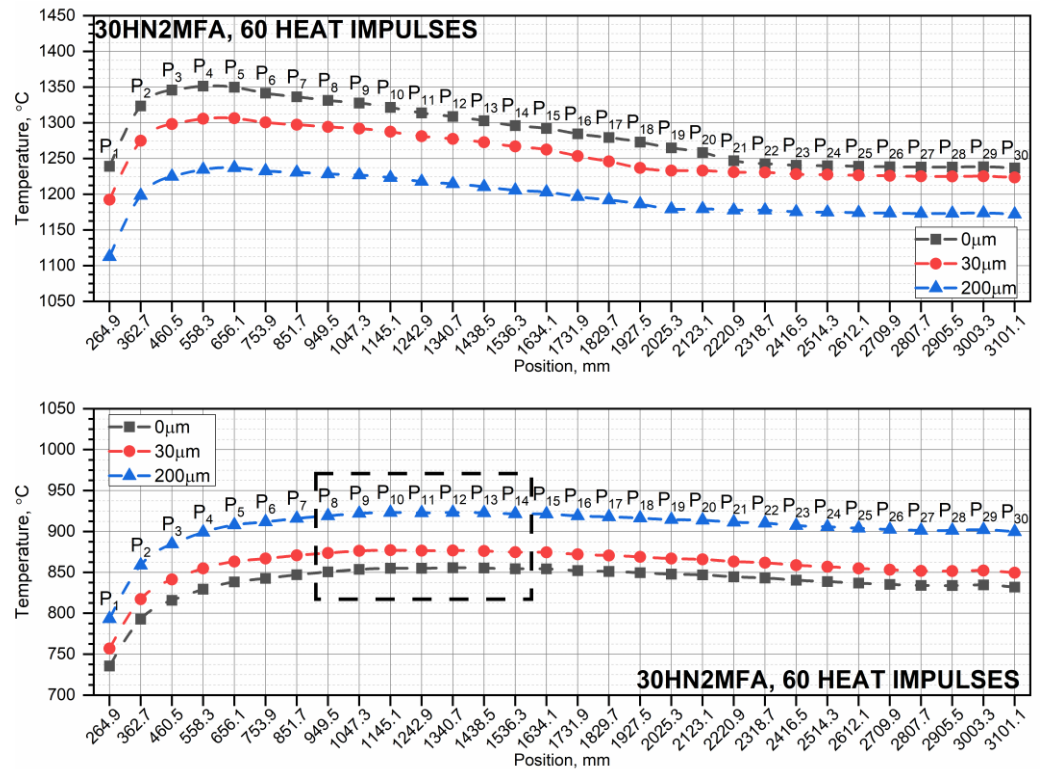


Figure 12. The highest peak temperatures (**upper figure**) and the lowest peak base temperatures (**lower figure**) for the considered cross-sections for 60 heat impulses.

3.2. Temperature Distribution in the X37CrMoV5-1 Tube for a Series of Ten, Thirty, and Sixty Heat Impulses

The temperature values $T_i(t, r, z)$ along the wall thickness of the tube for X37CrMoV5-1 steel with different chromium layer thicknesses, i.e., 0, 30, and 200 μm, at zone S30 for the sequence of sixty heat impulses are presented in Figure 13. In the case of X37CrMoV5-1 steel, material shrinkage occurs at a temperature of 870 °C. This temperature is exceeded to a depth of up to 0.5 mm at different times, depending on the thickness of the chromium layer on the inner surface of the tube. The fastest exceedance of the phase transformation temperature for a tube made of X37CrMoV5-1 steel will occur for the variant with a chromium layer of 200 μm. This means that the tube with 200 μm Cr will be exposed to the highest wear. After 4.9 s, i.e., after 49 heat impulses, zone S30 will exceed the phase transition temperature—Figure 13.

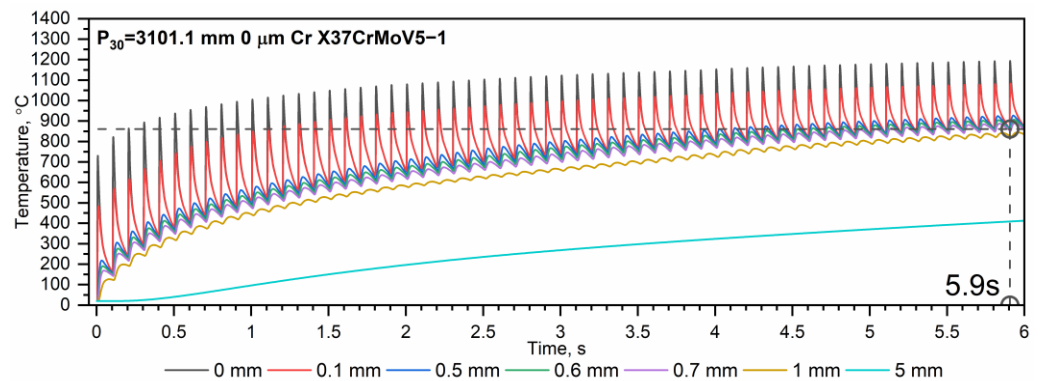


Figure 13. Cont.

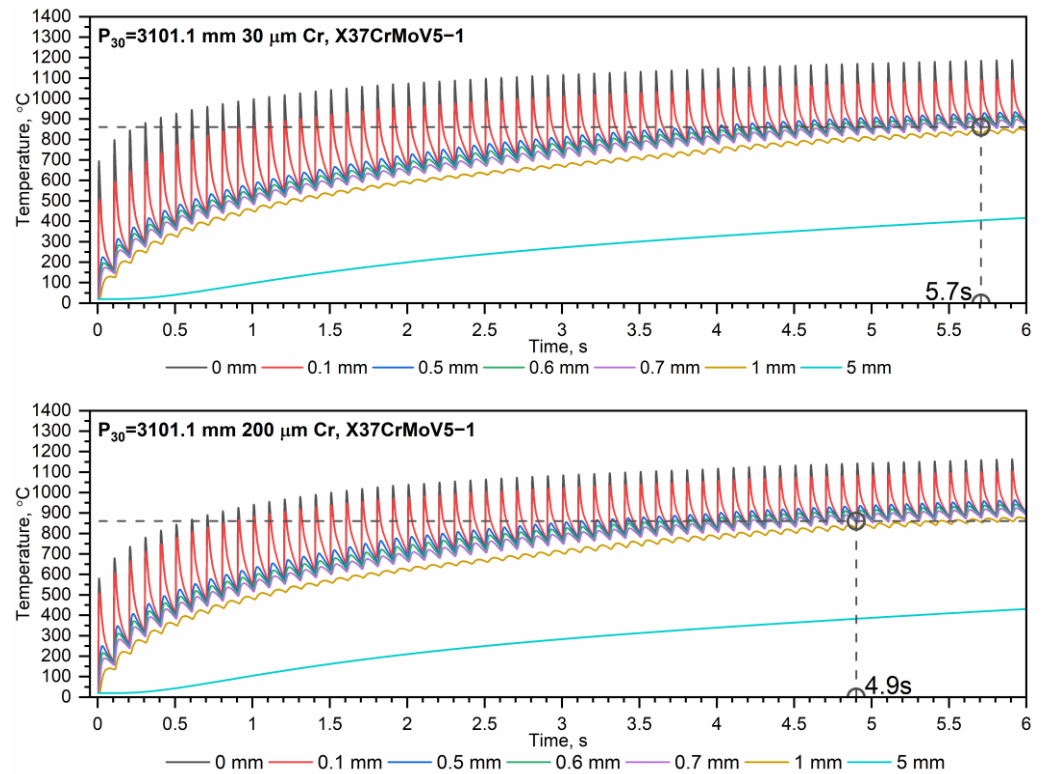


Figure 13. Temperature change $T_i(t, r, z)$ in the S30 zone for a series of 60 heat impulses for different depths from the inner surface of the tube, for X37CrMoV5-1 steel. The colored lines indicate the depth from the inner surface of the tube according to the graph legend.

The envelopes of the lowest peak base temperatures (the bottom curves in each drawing) and the highest peak temperatures (the top curves in each drawing) of the inner surface of the tube with different thicknesses of Cr (0, 30, and 200 μm) at the chosen six zones, i.e., S4, S10, S16, S21, S25, and S30, for 60 heat impulses are shown in Figure 14. In zones 4, 10, and 16, the highest peak temperatures are similar, and after 60 heat impulses, they are a little higher than 1300 $^{\circ}\text{C}$, when the temperatures in zones 21, 25, and 30 are little below 1300 $^{\circ}\text{C}$. However, for the lowest peak base temperatures, in all zones, after 60 heat impulses, the temperatures are close to 850 $^{\circ}\text{C}$.

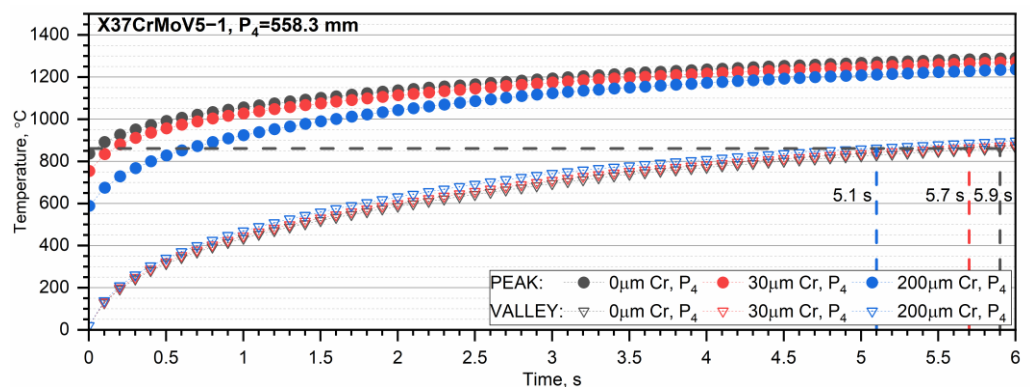


Figure 14. Cont.

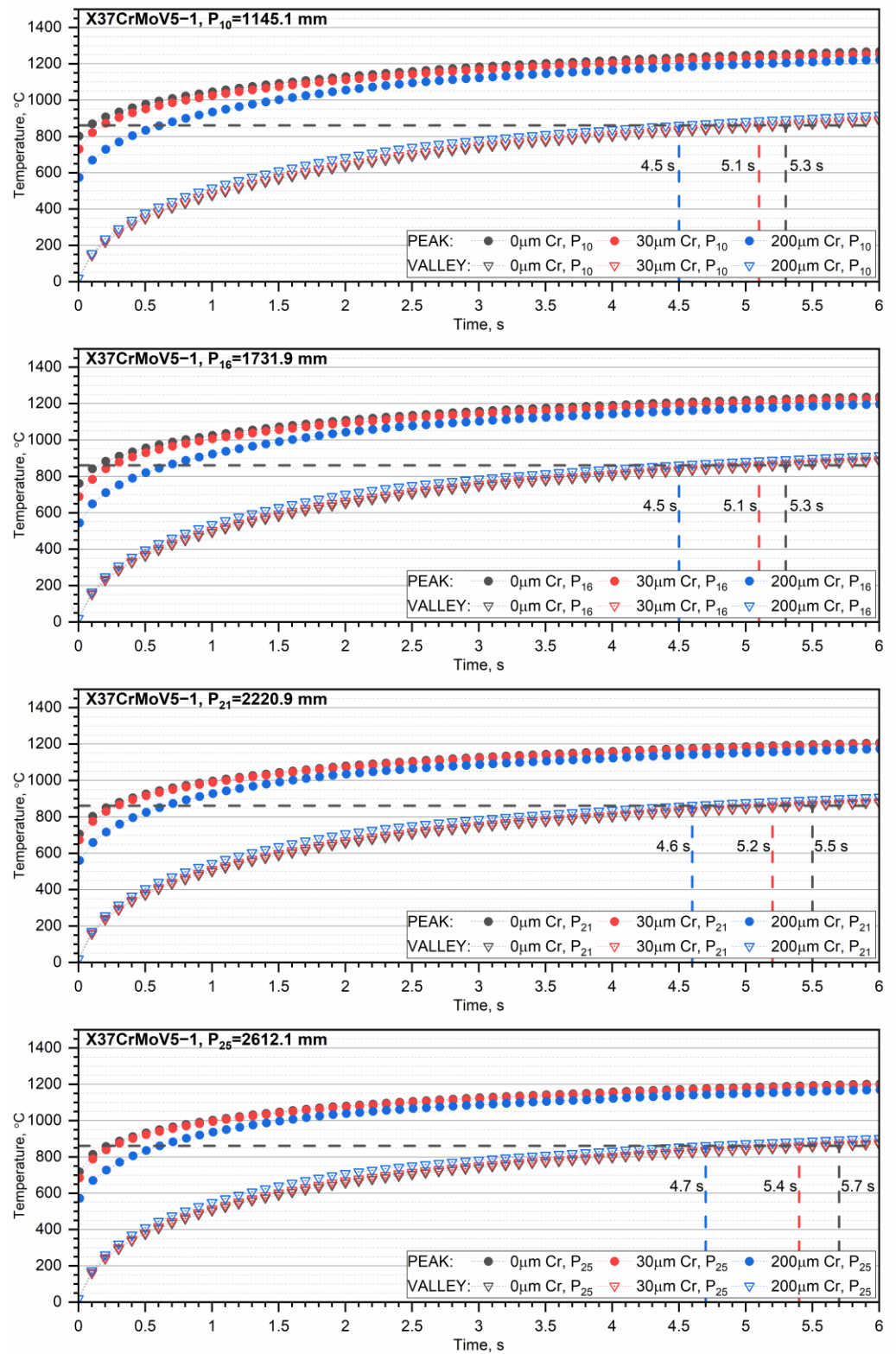


Figure 14. Cont.

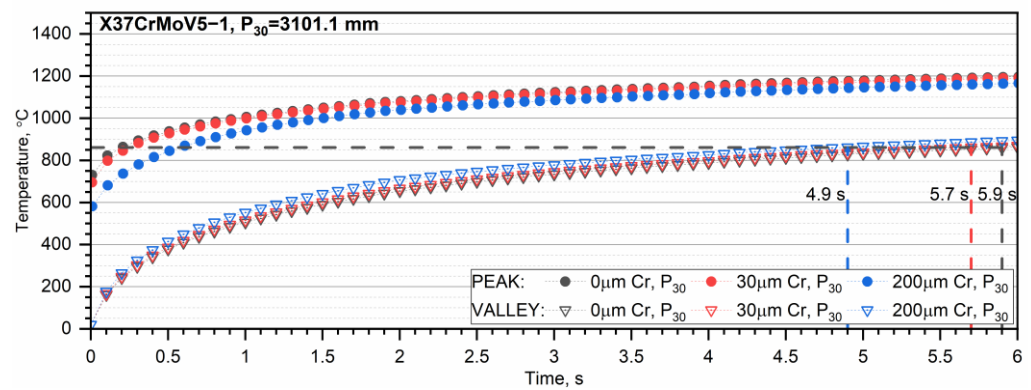


Figure 14. Envelopes of the lowest peak base temperatures (VALLEY) and the highest peak temperatures (PEAK) of the inner surface for 60 heat impulses.

The highest peak temperatures and the lowest peak base temperatures along the tube length with different chromium layers after 10, 30, and 60 heat impulses are presented in Figures 15–17. After 10 heat impulses, the maximum of the lowest peak base temperature is in the S27–S30 zones (Figure 15). After 30 heat impulses, the lowest peak base temperatures reach a maximum in zones S14–S22 (Figure 16), and after 60 heat impulses, they reach a maximum in zones S8–S14 (Figure 17).

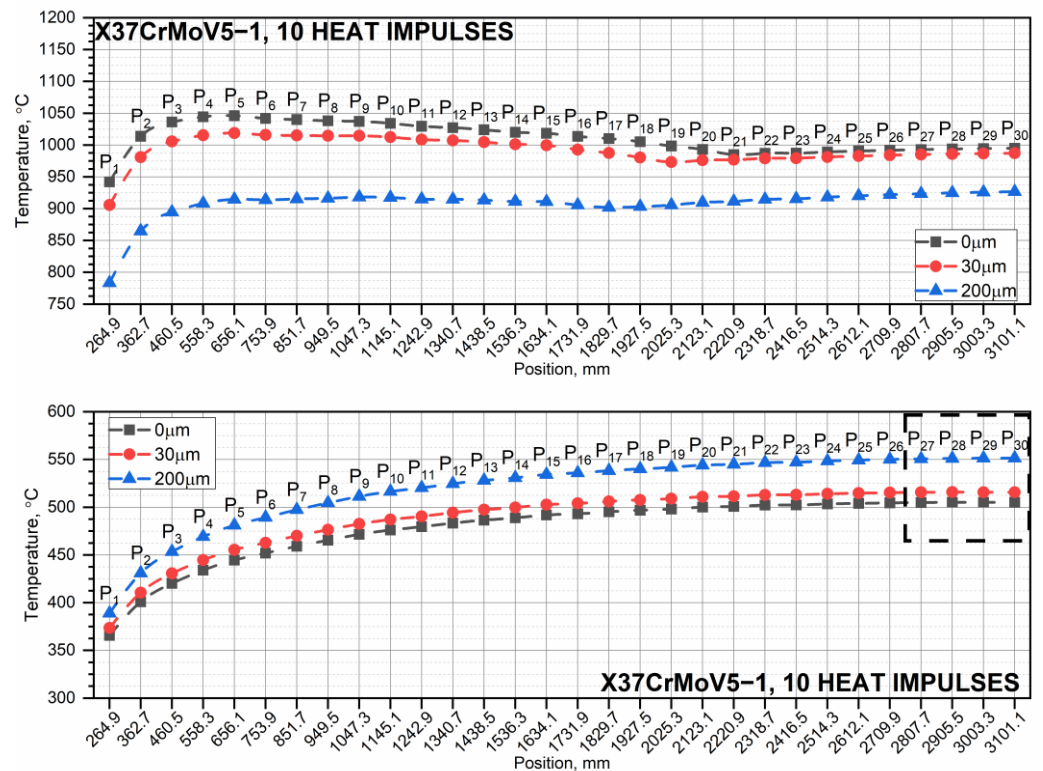


Figure 15. The highest peak temperatures (upper figure) and the lowest peak base temperatures (lower figure) for the considered cross-sections for 10 heat impulses.

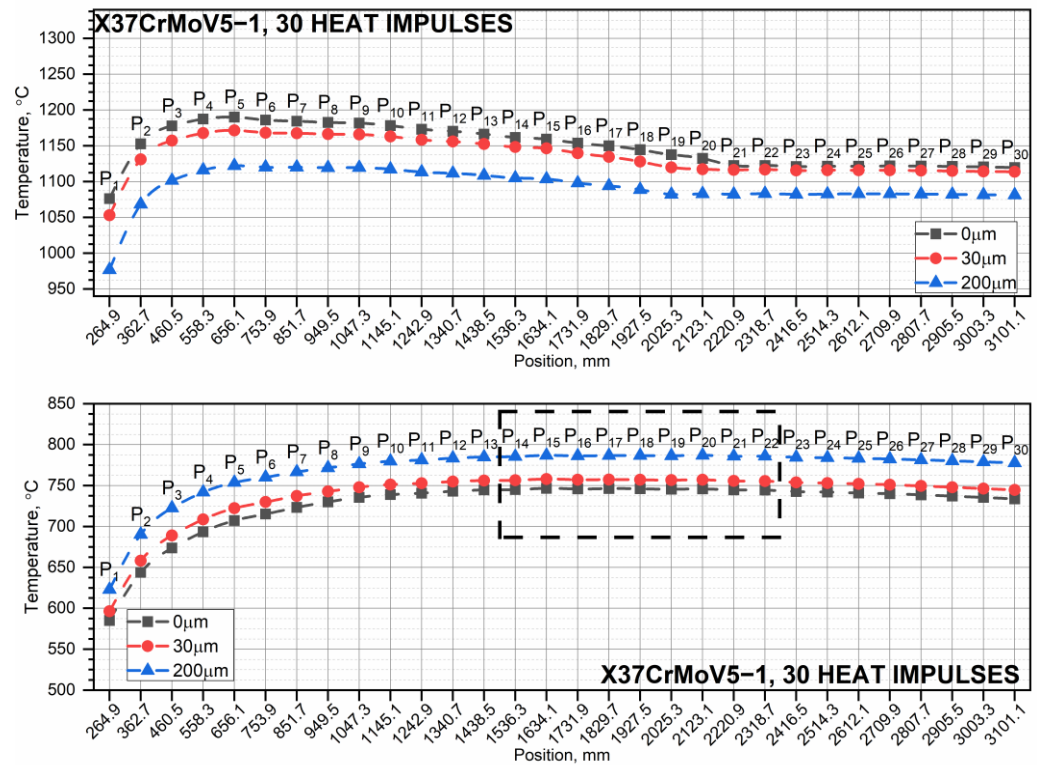


Figure 16. The highest peak temperatures (**upper figure**) and the lowest peak base temperatures (**lower figure**) for the considered cross-sections for 30 heat impulses.

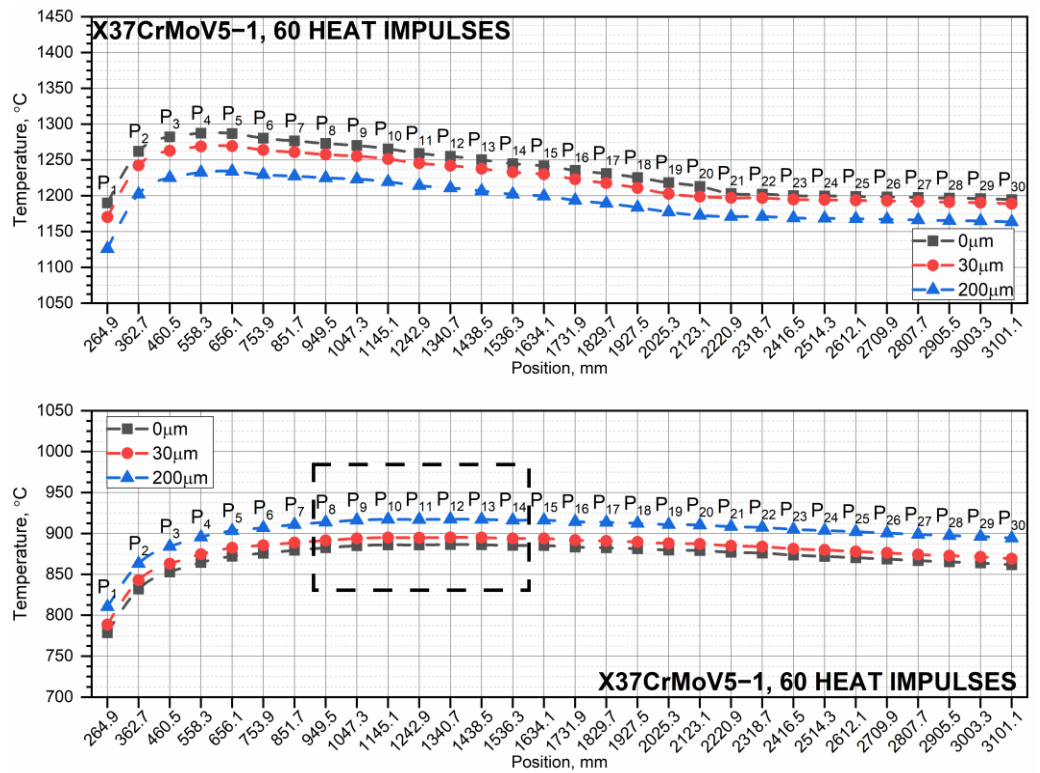


Figure 17. The highest peak temperatures (**upper figure**) and the lowest peak base temperatures (**lower figure**) for the considered cross-sections for 60 heat impulses.

4. Discussion

In this study, the influence of the type of steel with different shrinkage temperatures on heat transfer in the steel tube wall was examined. Calculations were carried out for two selected steels with clearly different shrinkage temperatures, i.e., 30HN2MFA and XCrMoV5-1. In 30HN2MFA steel, the shrinkage effect occurred at a temperature of approx. 750 °C, while in X37CrMoV5-1 steel, it occurred at a temperature of approx. 860 °C.

The number of thermal impulses necessary to obtain the shrinkage temperature on the inner surface of the tube, in the chosen zones 4, 10, 16, 21, 25, and 30, for both steels is summarized in Table 3 and presented in Figures 9 and 14. Regardless of the chromium layer thickness, for X37CrMoV5-1 steel, the number of thermal impulses necessary to obtain the shrinkage temperature is on average 20 thermal impulses higher than for 30HN2MFA steel. In the case of both steels, the inner surface without the chrome coating heats up to the shrinkage temperature the slowest, i.e., for 30HN2MFA steel, after 3.9 s (Figure 8), and for X37CrMoV5-1 steel, after 5.9 s (Figure 13). The shrinkage temperature is reached the fastest by a tube with a 200 µm thick chrome layer, i.e., for 30HN2MFA steel, after 2.7 s (Figure 8), and for X37CrMoV5-1 steel, after 4.9 s (Figure 13). Such a tube wears out the fastest. The thickness of the chromium layer also affects the highest peak temperatures on the inner surface of the pipe. As the layer thickness increases, the highest peak temperatures decrease and the lowest peak base temperatures increase—Figures 8, 9, 13 and 14.

Table 3. The number of heat impulses needed to obtain the shrinkage temperature on the inner surface of the tube in zones 4, 10, 16, 21, 25, and 30.

Zone	Steel Grade	Temperature of Shrinkage	Number of Heat Impulses for Different Chromium Layers		
			0 µm Cr	30 µm Cr	200 µm Cr
S4	30HN2MFA	741 °C	42	39	33
	X37CrMoV5-1	860.9 °C	59	57	51
S10	30HN2MFA	741 °C	37	33	27
	X37CrMoV5-1	860.9 °C	53	51	45
S16	30HN2MFA	741 °C	36	32	23
	X37CrMoV5-1	860.9 °C	53	51	45
S21	30HN2MFA	741 °C	36	33	26
	X37CrMoV5-1	860.9 °C	55	52	46
S25	30HN2MFA	741 °C	38	34	26
	X37CrMoV5-1	860.9 °C	57	54	47
S30	30HN2MFA	741 °C	39	35	27
	X37CrMoV5-1	860.9 °C	59	57	49

As the number of successive thermal impulses increases, the maximum temperature of the inner surface moves from the end of the tube, i.e., from the tube outlet, to its beginning—Figures 10–12 and 15–17 (lower figures). For both steels, the maximum temperatures of the inner surface occur in the same zones, i.e., for 10 thermal impulses, in zones S27–S30, for 30 thermal impulses, in zones S14–S22, and for 60 thermal impulses, in zones S8–S14.

5. Conclusions

Simulations were conducted to study heat transfer in a tube with a chrome layer on its inner surface. The simulations took into account temperature-dependent thermophysical parameters for both types of steel and chrome. To calculate the temperature as a function of time along the entire length of the tube, it was divided into 30 parts. The calculations were completed in a relatively short time, i.e., for 60 thermal impulses, in about 6 h. The following is a summary of the results obtained from a numerical simulation of heat transfer

in a tube with varying thicknesses of chrome layer (0 μm , 30 μm , and 200 μm) on its inner surface:

- (1) Repeatedly exceeding the shrinkage temperature during the operation of the device is an unfavorable phenomenon because it causes cracks in the steel on the inner surface of the tube and, as a result, the peeling of the chrome layer.
- (2) When the pipe is operated with successive thermal impulses, it can be seen that as the thickness of the chrome layer increases, the temperature of the inner surface of the pipe increases. This is due to the high thermal conductivity of chromium. The number of thermal impulses needed to obtain the shrinkage temperature on the inner surface of the pipe is the largest for a pipe without a chrome coating.
- (3) A steel tube with a higher shrinkage temperature wears out more slowly because more heat impulses are needed to reach this temperature. In the case of a pipe made of X37CrMoV5-1 steel, regardless of the zone, the number of thermal impulses needed to reach the shrinkage temperature is significantly higher compared to a tube made of 30HN2MFA steel, i.e., by approx. 20 heat impulses. It is usually recommended that the number of heat impulses for the continuous operation of the tube should not exceed 30 heat impulses.
- (4) The smaller the thickness of the chromium layer on the inner surface, the greater the number of heat impulses needed to reach the shrinkage temperature of the steel. This is particularly important for a 30HN2MFA steel tube, for which the shrinkage temperature is reached after approx. 30 heat impulses.
- (5) As the number of successive thermal impulses increases, the maximum temperature of the inner surface of the tube, i.e., the lowest peak base temperature, moves from the end of the tube, i.e., from the tube outlet, to its beginning. This is due to the greater thickness of the tube wall in its initial part, which results in heat accumulation for a large number of thermal impulses.

Author Contributions: Conceptualization, M.Z., P.K. and Z.S.; methodology, P.K., M.Z. and Z.S.; software, M.Z. and Z.S.; validation, P.K. and M.Z.; formal analysis, P.K., M.Z. and Z.S.; writing—original draft preparation, P.K., M.Z. and Z.S.; writing—review and editing, P.K., M.Z. and Z.S. All authors have read and agreed to the published version of the manuscript.

Funding: The methods and results presented in the paper were obtained thanks to funding from the university research project UGB-821 of the Military University of Technology, in 2023 (Warsaw, PL), entitled “Numerical simulations of heat transfer in the barrel of a 30HN2MFA steel cannon, the inner surface of which was covered with a layer of chromium of various thicknesses. Complementary tests of thermophysical properties of Maraging 350 and WCL steels”.

Data Availability Statement: Data are contained within the article.

Conflicts of Interest: The authors declare no conflicts of interest.

References

1. Sopok, S.; Rickard, C.; Dunn, S. Thermal–chemical–mechanical gun bore erosion of an advanced artillery system part one: Theories and mechanisms. *Wear* **2005**, *258*, 659–670. [[CrossRef](#)]
2. Sopok, S.; Rickard, C.; Dunn, S. Thermal–chemical–mechanical gun bore erosion of an advanced artillery system part two: Modeling and predictions. *Wear* **2005**, *258*, 671–683. [[CrossRef](#)]
3. Lawton, B. Thermo-chemical erosion in gun barrels. *Wear* **2001**, *251*, 827–838. [[CrossRef](#)]
4. Ebihara, W.T.; Rorabaugh, D.T. Mechanisms of Gun-Tube Erosion and Wear. In *Gun Propulsion Technology*; Stiefel, L., Ed.; American Institute of Aeronautics and Astronautics: Washington, DC, USA, 1988; pp. 357–376, ISBN 0930403207.
5. Ahmad, I. The Problem of Gun Barrel Erosion: An Overview. In *Gun Propulsion Technology*; Stiefel, L., Ed.; American Institute of Aeronautics and Astronautics: Washington, DC, USA, 1988; pp. 311–356, ISBN 0930403207.
6. Baracuti, A.J. Wear-Reduction Additives—Role of Propellant. In *Gun Propulsion Technology*; Stiefel, L., Ed.; American Institute of Aeronautics and Astronautics: Washington, DC, USA, 1988; pp. 377–412, ISBN 0930403207.
7. Almotairi, A.; Farhat, Z.; Warkentin, A. Thermal damage of conventional hard chromium coatings on 416 stainless steel. *Eng. Fail. Anal.* **2019**, *105*, 1118–1130. [[CrossRef](#)]

8. Mills, K.C.; Su, Y.; Li, Z.; Brooks, R.F. Equations for the Calculation of the Thermo-physical Properties of Stainless Steel. *ISIJ Int.* **2004**, *44*, 1661–1668. [[CrossRef](#)]
9. Zhen, W.; Jin, W. Heat Transfer Simulation of Large Caliber Gun Barrel. *IOP Conf. Ser. Earth Environ. Sci.* **2020**, *546*, 42039. [[CrossRef](#)]
10. Koniorczyk, P.; Zmywaczyk, J.; Dębski, A.; Zieliński, M.; Preiskorn, M.; Sienkiewicz, J. Investigation of Thermophysical Properties of Three Barrel Steels. *Metals* **2020**, *10*, 573. [[CrossRef](#)]
11. Moravčík, R.; Štefániková, M.; Čička, R.; Čaplovič, L.; Kocúrová, K.; Šturm, R. Phase Transformations in High Alloy Cold Work Tool Steel. *SV-JME* **2012**, *58*, 709–715. [[CrossRef](#)]
12. Balaško, T.; Burja, J.; Medved, J. Effect of steel's thermal condition on the transformation temperatures of two hot-work tool steels with increased thermal conductivity. *Mater. Technol.* **2023**, *57*, 617–626. [[CrossRef](#)]
13. Dębski, A.; Surma, Z.; Koperski, W. *Material and Technological Optimization Research in Terms of Increasing the Durability of Small Arms*; Military University of Technology: Warsaw, Poland, 2009.
14. Woźniak, R.; Torecki, S.; Leciejewski, Z. *Technology Demonstrator of a Remotely Controlled 35 mm Anti-Aircraft System*; Military University of Technology: Warsaw, Poland, 2011.
15. Huang, X.; Conroy, P.; Carter, R. 5.56 mm Ceramic Gun Barrel Thermal Analysis with Cycled Ammunition. In Proceedings of the 23rd International Symposium on Ballistics, Tarragona, Spain, 16–20 April 2007; pp. 16–20.
16. Loiola, B.R.; Susantez, Ç.; Caldeira, A.B. Numerical modelling of heat transfer and simulation of a 5.56 mm rifle barrel. *J. Phys. Conf. Ser.* **2023**, *2478*, 112030. [[CrossRef](#)]
17. Zieliński, M.; Koniorczyk, P.; Surma, Z.; Zmywaczyk, J.; Preiskorn, M. Numerical Study of Heat Transfer in a Gun Barrel Made of Selected Steels. *Energies* **2022**, *15*, 1868. [[CrossRef](#)]
18. Zieliński, M.; Koniorczyk, P.; Surma, Z. Studies on Influence of Chromium Layer on Inner Surface of Steel Tube on Heat Transfer. *Appl. Sci.* **2023**, *13*, 5523. [[CrossRef](#)]
19. Mishra, A.; Hameed, A.; Lawton, B. A Novel Scheme for Computing Gun Barrel Temperature History and Its Experimental Validation. *J. Press. Vessel. Technol.* **2010**, *132*, 444. [[CrossRef](#)]
20. Keith Clutter, J.; Shyy, W. Computation of High-Speed Reacting Flow for Gun Propulsion Applications. *Numer. Heat Transf. Part A Appl.* **1997**, *31*, 355–374. [[CrossRef](#)]
21. Wu, Y.-H. Analysis of the Temperature Field of a Gun Tube Based on Thermal-Solid Coupling. *RJASET* **2013**, *5*, 4110–4117. [[CrossRef](#)]
22. Akçay, M.; Yükselen, M.A. Unsteady Thermal Studies of Gun Barrels During the Interior Unsteady Thermal Studies of Gun Barrels during the Interior Ballistic Cycle with Non-Homogenous Gun Barrel Material Thermal Characteristics. *J. Therm. Sci. Technol.* **2014**, *34*, 75–81.
23. Ding, C.; Liu, N.; Zhang, X. A mesh generation method for worn gun barrel and its application in projectile-barrel interaction analysis. *Finite Elem. Anal. Des.* **2017**, *124*, 22–32. [[CrossRef](#)]
24. Hill, R.; McLeod, L. Methodology for Transient Thermal Analysis of Machine Gun Barrels Subjected to Burst Firing Schedules. Available online: <https://nts.com/content/uploads/2017/12/Methodology-for-Transient-Thermal-Analysis-of-Machine-Gun-Barrels-Subjected-to-Burst-Firing-Schedules.pdf> (accessed on 2 November 2023).
25. Hill, R.D.; Conner, J.M. Transient Heat Transfer Model of Machine Gun Barrels. *Mater. Manuf. Process.* **2012**, *27*, 840–845. [[CrossRef](#)]
26. Ho, C.Y.; Powell, R.W.; Liley, P.E. Journal of Physical and Chemical Reference Data: Thermal Conductivity of the Elements: A Comprehensive Review. Available online: <https://srd.nist.gov/JPCRD/jpcrdS1Vol3.pdf> (accessed on 2 November 2023).
27. McBride, B.J.; Gordon, S.; Reno, M.A. NASA Technical Paper 3287: Thermodynamic Data for Fifty Reference Elements. Available online: <https://ntrs.nasa.gov/api/citations/20010021116/downloads/20010021116.pdf> (accessed on 2 November 2023).
28. Chromium Thermal Properties from Material Properties Database (MPDB) by JAHAM Software. Available online: https://www.jaham.com/demo_version.html (accessed on 2 November 2023).
29. Koniorczyk, P.; Zieliński, M.; Sienkiewicz, J.; Zmywaczyk, J.; Dębski, A. Experimental Studies of Thermophysical Properties and Microstructure of X37CrMoV5-1 Hot-Work Tool Steel and Maraging 350 Steel. *Materials* **2023**, *16*, 1206. [[CrossRef](#)]
30. Bejan, A.; Kraus, A.D. *Heat Transfer Handbook*; Wiley: Hoboken, NJ, USA, 2003; ISBN 0471390151.

Disclaimer/Publisher's Note: The statements, opinions and data contained in all publications are solely those of the individual author(s) and contributor(s) and not of MDPI and/or the editor(s). MDPI and/or the editor(s) disclaim responsibility for any injury to people or property resulting from any ideas, methods, instructions or products referred to in the content.